Evolution of Correlated Morphological and Structural Disorder in Boehmite-Derived Alumina with Progressive Calcination

Nivedita Sudheer, Sharmin Sharna, Virgile Rouchon, Dris Ihiawakrim, Marc Lenertz, Pierre Levitz, Pierre Rabu, Ovidiu Ersen

ChemCatChem

Research Article
doi.org/10.1002/cctc.202400677

Chemistry Europe
European Chemical Societies Publishing

www.chemcatchem.org

Evolution of Correlated Morphological and Structural Disorder in Boehmite-Derived Alumina with Progressive Calcination

Nivedita Sudheer,[a, b] Sharmin Sharna,[a] Virgile Rouchon,[b] Dris Ihiawakrim,[a] Marc Lenertz,[a] Pierre Levitz,[c] Pierre Rabu,[a] and Ovidiu Ersen*[a]

This study explores the morphological and structural transformation of boehmite (AlOOH) into transition aluminas during calcination, a pathway crucial for diverse industrial applications. The primary focus is on the topotactic transformation of boehmite into γ-Al_2O_3 and its subsequent transitions into higher temperature polymorphs, culminating in α-Al_2O_3. Utilizing a combination of *in situ* X-ray diffraction, *in situ* and *ex situ* transmission electron microscopy, ^{27}Al solid-state nuclear magnetic resonance, thermogravimetric analysis, nitrogen physisorption, and mercury porosimetry, this work provides insights into the morphological and structural reordering during the calcination process. Furthermore, the study highlights the significant impact of thermal processing on the morphological evolution of boehmite and transition aluminas, characterized by changes in pore structure sizes and shapes. These findings offer valuable insights for optimizing the properties of alumina-based materials for specific applications.

Introduction

Boehmite (AlOOH) is extensively employed in industrial catalysis, where it undergoes conversion to γ-alumina and serves as a support material for dispersing active catalytic phase.[1,2] The attributes of surface area, porosity, and porous network are of paramount importance in catalytic processes, particularly regarding the dispersion of the active phase and the diffusion of reactant and product molecules. These properties are predominantly impacted by the inherent characteristics of boehmite and its processing conditions towards alumina.[3–5] The transformation of boehmite to alumina through calcination is a widely employed method in various industrial sectors.[6] The process of transformation entails a pseudomorphic topotactic transformation, whereby the morphology and structure of AlOOH are transferred to γ-Al_2O_3.[7,8] Several types of alumina polymorphs possess unique physicochemical properties that may influence their stability and interaction with the active phase.[9,10] Furthermore, catalysts are subjected to elevated temperatures and varying gaseous and/or liquid environment during catalytic reactions, which may trigger phase alterations. A particular concern arises when the alumina support undergoes a phase transition to α-Al_2O_3, leading to a decrease in surface area and porosity, together with the modification of the surface chemistry thereby affecting the catalytic activity.[11]

The transformation of boehmite into alpha alumina is a multifaceted process involving a series of transitional aluminas, namely γ-Al_2O_3, δ-Al_2O_3, Θ-Al_2O_3, culminating in α-Al_2O_3.[12,13] The sequence of transitions is significantly impacted by various factors, including the synthesis pathway, crystallinity, heating rate, presence of impurities, moisture content.[9,10,14–18] The initial step of boehmite dehydration to γ- Al_2O_3 is pseudomorphic, with a topotactic relation. The crystallographic orientation relationships between γ-AlOOH and γ-Al_2O_3 have been extensively investigated for over five decades.[7,8,19,20] The subsequent transitions towards higher temperature polymorphs gradually restores structural order from an initial low temperature highly disordered γ-Al_2O_3 phase. The primary structural differences among these polymorphs are related to the disposition of aluminum cations within the interstitial voids of an approximately cubic close-packed oxygen anion array.[21–27]

In this context, understanding the bulk and surface characteristics of γ-Al_2O_3 remains challenging due to inconsistencies in the reported structures and levels of disorder.[28–32] These discrepancies are partly due to variations in the initial boehmite's characteristics (crystallinity, purity, crystallite size and morphology) and the thermal treatment (time, temperature, moisture content) which result in varying degrees of transformation among the transition alumina polymorphs. Significant attention has been given to refining the crystalline structure of γ-Al_2O_3 through experimental and computational methods, yet consensus is still lacking. Conversely, the mesoscopic evolution of crystallites has only been sporadically

[a] N. Sudheer, S. Sharna, D. Ihiawakrim, M. Lenertz, P. Rabu, Prof. O. Ersen
Institut de Physique et Chimie des Matériaux de Strasbourg (IPCMS), UMR 7504 CNRS – Université de Strasbourg, 23 Rue du Loess, 67200 Strasbourg, France
E-mail: ovidiu.ersen@ipcms.unistra.fr

[b] N. Sudheer, V. Rouchon
IFP Energies nouvelles (IFPEN), Lyon Establishment, Rond-Point de l'Echangeur de Solaize, BP 3-69360 Solaize, France

[c] P. Levitz
Physicochimie des Electrolytes et Nanosystèmes interfaciaux Laboratory (PHENIX), CNRS and University Pierre et Marie Curie, 75252 Paris cedex 5, France

investigated, with studies showing a strong correlation between the formation and evolution of intracrystalline pores and the structural evolution of the phases.[33–35] The diffusion of protons, hydroxyls, water and aluminum ions are competing processes required to dehydrate the structure and compensate for the local charge change.[34,36] This competition leads to a failure in achieving a purely ordered oxide phase, resulting in a highly disordered, defective spinel-like structure where tetrahedrally coordinated aluminums atoms are charge-compensated by protons. This structural disorder causes morphological changes at the nanocrystallite scale that deviate from the ideal topotactic/pseudomorphic representation, where nanoscopic voids represent the non-fully compensated structure "collapse".[1,34] Subsequent thermal processing generally induces a further morphological evolution in pore numbers, sizes, and shapes.

To date, such observations have primarily been made by *ex situ* electron microscopy and textural analyses on micrometer-sized crystals.[34,36,37] There is currently no experimental evidence documenting *in situ* transformations in nanometer-sized crystallites, which better emulate real catalytic supports. Our study focuses on the morphological evolution of boehmite and transition aluminas by thermal processing, combining *in situ* X-ray diffraction (XRD) and *in situ* transmission electron microscopy (TEM) on boehmite powders characterized by 40 nm sized crystallites. These *in situ* studies are supported by ^{27}Al nuclear magnetic resonance (solid state-NMR), thermogravimetric analysis (TGA), N_2 physisorption, Hg-porosimetry and *ex situ* TEM. Together, these methods aim to provide insights into the mechanisms governing correlated progressive morphological and structural ordering.

Materials and Methods

Materials: High purity boehmite (AlOOH) powder with an average particle size of 35 μm was supplied by Sasol Inorganics Germany. The chemical impurities are as follows: C content is 0.25 %, SiO_2 content ranges from 0.01 % to 0.015 %, and Fe_2O_3 content ranges from 0.005 % to 0.015 %.[38]

***In situ* X-ray Diffraction**: XRD measurements were carried out on a D8 Discover diffractometer in Bragg-Brentano geometry, equipped with a Cu sealed tube ($\lambda_{K\alpha1} = 0.15406$ nm), a quartz front monochromator, and an energy-resolved Lynxeye XE-T linear detector. The diffractometer is equipped with an Anton Paar HTK 1200 N temperature chamber, allowing temperature dependent measurement from 25 to 1200 °C. The scanning range encompassed 10 to 80 degrees of 2θ. The specimen underwent a thermal ramping of 5 °C/min and kept at constant temperature for half an hour for each XRD measurement. Measurements were taken at room temperature, then at 200 °C, and up to 1200 °C with 50 °C steps. Eight successive measurements were realized at 1200 °C (4 hours) to study any further sample evolution.

Thermal analysis: The thermogravimetric/differential thermal analysis (TG/DTA) was simultaneously carried out using a SDT Q600 from TA Instruments. A 50 mg of sample was placed in an alumina crucible and subjected to heating at a rate of 10 °C/min in the presence of a nitrogen atmosphere (20 ml/min) and air (30 ml/min).

***In situ* Scanning Transmission Electron Microscopy (in situ STEM)**: The *in situ* STEM experiments were conducted using a spherical aberration-corrected JEOL JEM-2100F microscope with an acceleration voltage of 200 kV. An "Atmosphere system" by Protochips™ was used for the *in situ* experiments. The system comprises a special sample holder, SiC-based microelectromechanical system (MEMS) support E-chips to confine the sample, an automated gas manifold, and a Clarity Workflow software package. The powdered sample was suspended in ethanol and simply drop-cast onto the heating chip. All the *in situ* observations were conducted under air at 1 atm pressure. The temperature was gradually increased from ambient temperature to 100 °C at a heating rate of 10 °C/min, and maintained at this temperature for 60 min. Subsequently, the temperature was increased to 450 °C at the same heating rate. After this, the temperature was increased by 50 °C increments, maintaining each increment for 30 mins, until reaching the final temperature of 1000 °C.

***Ex situ* transmission electron microscopy**: *Ex situ* STEM imaging and electron diffraction were performed using the same microscope, as well as a JEOL cold FEG F200 microscope operated under similar conditions. The samples were prepared by suspending in ethanol and drop-casting onto 3 mm holey carbon coated Cu grids.

Mercury porosimetry: The analyses were conducted using AutoPore IV equipment from Micromeritics. The samples were treated for 2 hours at 250 °C. Intrusion curves were measured up to a maximum pressure of 400 MPa using a mercury surface tension of 485 dyne/cm and a contact angle of 140°.

Nitrogen Physisorption: The analyses were performed in a ASAP 2420 apparatus from Micrometrics. To remove any physisorbed species from the sample surface, the samples were pretreated at 350 °C for 3 hours under secondary vacuum (10^{-6} mm Hg).

^{27}Al NMR: The samples were analyzed using MAS NMR of aluminum 27 with a 4 mm MQMAS probe on an Avance 400 spectrometer from Bruker operating at 12 kHz spinning speed and 9.4 T magnetic field. The ^{27}Al NMR spectra were obtained using a single-pulse MAS sequence under selective conditions (low radio-frequency field, approximately 25 kHz) and quantitative conditions (low pulse angle equal to $\pi/22$ corresponding to a pulse duration of 1 μs). The recycling time (d1) is 0.5 s and the analysis comprised 8192 scans, totaling 1 h 15 min. Chemical shifts were referenced to $Al(NO_3)_3$, ($\delta = 0$ ppm). Quantitative extraction of the proportions of Al^{VI} and Al^{IV} coordination was computed as the normalized integrals within chemical shift ranges of −50–25 ppm and 25–90 ppm, respectively. Reproducibility measurements for this procedure on alumina show deviations within ±1 % for both Al^{VI} and Al^{IV} coordination states.

Results

In situ thermal treatment were acquired using STEM, XRD, and TGA-DTA. For the *ex-situ* experiments, the unaltered boehmite underwent heating treatments of 3 hours at temperatures of 450 °C, 700 °C, 900 °C, and 1000 °C, as well as a 12-hour heat treatment at 1000 °C. These temperatures were chosen based on the expected transition temperatures of the alumina polymorphs.[39–41]

Figure 1 illustrates DTA and TGA curves during the heat treatment of the boehmite sample. The DTA diagram exhibits 3 discernible steps as marked on the curve. Step-I represents an endothermic event at a temperature of 55.5 °C which can be ascribed to the desorption of physically adsorbed water on the surfaces of AlOOH. Step–II pertains to the endothermic phase transformation of boehmite to the γ-Al_2O_3 phase, which takes

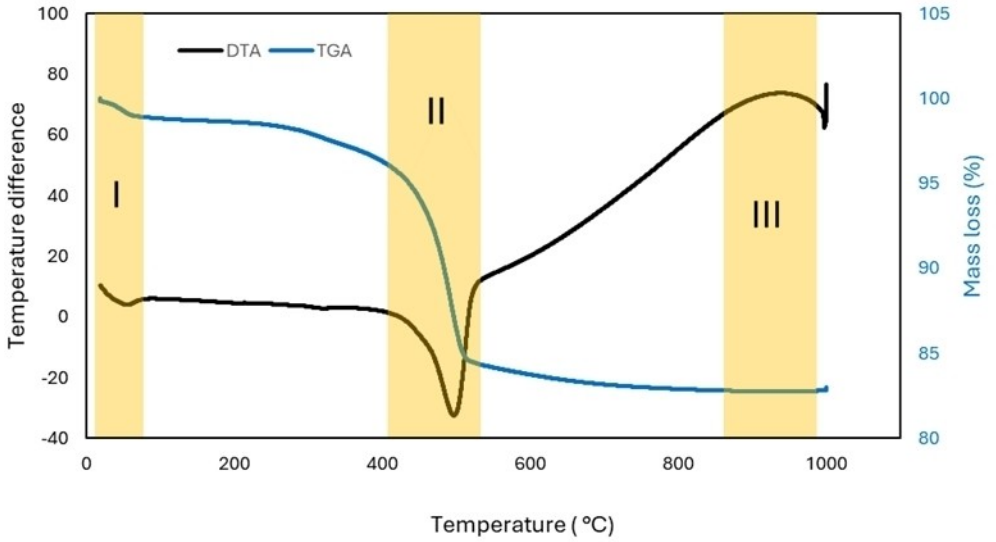

Figure 1. Differential thermal analysis (DTA) and thermogravimetric analysis (TGA) results obtained for the D40 boehmite grade using a heating rate of 10 °C/min.

place at a temperature of roughly 498 °C and results in a total weight reduction of approximately 15% according to the TGA graph. From 540 °C, a steady increase in temperature difference is observed, which is correlated to the gradual loss of hydroxyls from alumina, until a very broad peak (step-III) at about 850 °C. The broad peak can be attributed to the γ-Al_2O_3 to δ-Al_2O_3 phase transition as confirmed later by XRD. The peak at the end of the DTA curve (at 998 °C) is considered an anomaly in the data, as the heating was stopped at 1000 °C. Consequently, any peaks occurring near this temperature may not represent genuine thermal events but rather artifacts resulting from the cessation of heating.

The mercury porosimetry data for the initial boehmite sample indicate a pore size distribution centered at 43 nm, consistent with the expected intercrystallite pore space (Figure 2). Throughout the transition aluminas, the dominant pore size population remains at 43–45 nm. The tailing of this main distribution towards lower pore sizes, typically in the 10–30 nm range is highest for the 450 °C sample and decreases gradually for the samples calcined at higher temperature. Similarly, the lower end of the mesoporous domain (4–10 nm) shows an increased pore volume contribution for the 450 °C sample compared to boehmite, with variable contributions for the higher temperature polymorphs.

For the boehmite sample, nitrogen physisorption analysis indicates a BET specific surface area and mesoporous volume of 45 m^2/g and 0.34 cm^3/g, respectively (Table 1). The t-plot data processing indicates a very low microporous volume of 5.2×10^{-3} cm^3/g and a surface area of 12 m^2/g. The BJH desorption branch pore size distribution (PSD) shows a single population at 40 nm diameter. The BET surface area increases drastically for the 450 °C calcined sample up to 118 m^2/g. The specific surface area decreases for the samples calcined at higher temperatures, returning to 45 m^2/g for the 900 °C calcined sample, the value remains consistent even for the sample calcined at 1000 °C for 12 h. The mesoporous volume similarly increases to 0.43 cm^3/g for the 450 °C and the 700 °C steps and then decreases progressively to 0.37 cm^3/g over the 900 °C and 1000 °C steps (Figure 2). For the BET specific surface area the relative increase from boehmite to the 450 °C sample is 250%. The pore size distribution (PSD) from the BJH desorption branch remains constant at 40 nm until the first 1000 °C step where it increases to 49 nm.

As for the mercury porosimetry, the intermediate mesoporous pore size (10–30 nm) contribution in the PSD decreases gradually from the 450 °C step to the most severely calcined sample. In the lowest pore size range probed by N_2 physisorption (3–5 nm), a pore volume contribution is seen for samples

Table 1. ^{27}Al NMR, Hg porosimetry and N_2-physisorption data for the raw boehmite sample and different calcination stages. Al in tetrahedra (Td) and octahedral (Oh) coordination are given in relative percentage.

		Boehmite raw	450 °C-3 h	700 °C-3 h	900 °C-3 h	1000 °C-3 h	1000 °C-12 h
Al (Td)	%	–	31	32	32	33	32
Al (Oh)	%	100	69	68	68	67	68
S_{BET}	(m^2/g)	45.4	118.3	67.7	46.6	45.1	45.0
V_{meso}	(cm^3/g)	0.34	0.43	0.43	0.39	-	0.37
S_{micro}	(m^2/g)	12.0	34.0	7.0	4.0	6.0	7.0

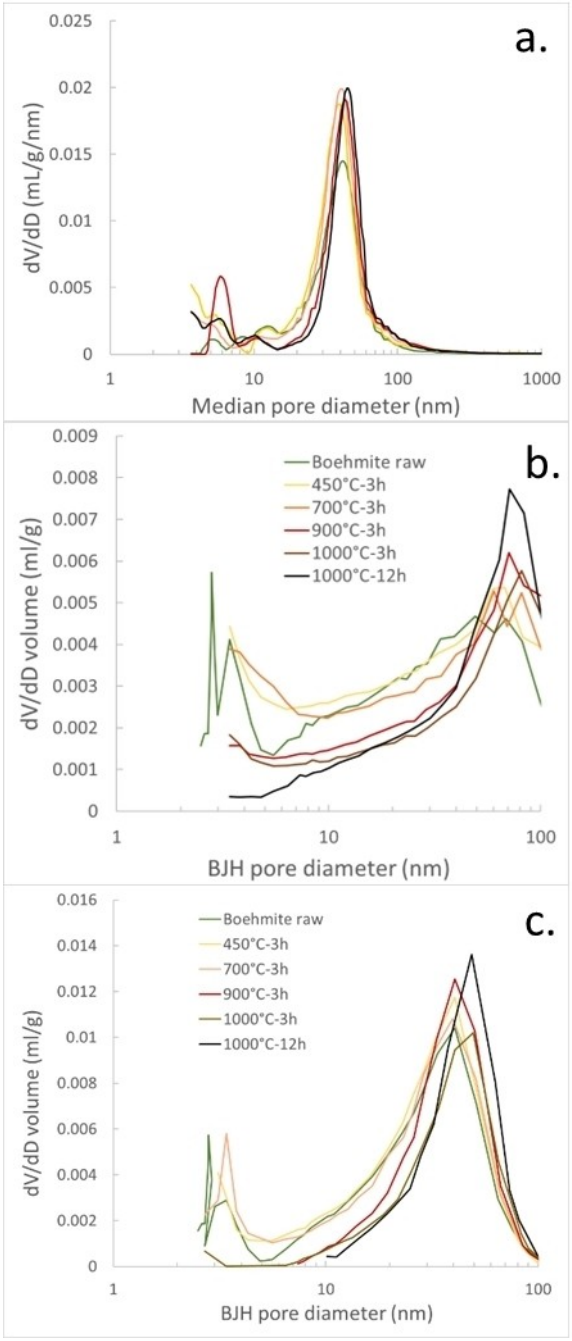

Figure 2. Textural analyses of the initial boehmite and variously calcined samples up to 1000 °C for 12 h. (a) Mercury porosimetry curves representing the normalized volume as a function of the pore size. (b) BJH calculation of the pore size distribution from the N_2 adsorption branch. (c) BJH calculation of the pore size distribution from the N_2 desorption branch.

calcined at temperatures lower than 900 °C, which disappears at higher temperatures.

The t-plot processing for the 450 °C calcined samples indicate a net increase in micropore specific surface area and volume of 280 %, compared to boehmite, which is comparable to BET results (Figure 3). The microporous volume falls to half the value of boehmite already at the 700 °C calcination step and remains in this range for the successive samples. The micro-porous specific surface area decreases from 34 cm^2/g at 450 °C to 4-7 cm^2/g for the most severely calcined sample.

The ^{27}Al MAS NMR spectrum of boehmite is characterized by a sharp single peak centered at 6 ppm characterizing the unique octahedral environment of aluminum in the boehmite structure. The 450 °C calcined sample is characterized by an octahedral peak centered at 6.8 ppm broadened more specifically towards negative chemical shifts, and the appearance of a broad peak centered at 64 ppm, characteristic of tetrahedrally coordinated aluminum. With further thermal treatment, the octahedral peak centered at 6.8 ppm gradually becomes thinner and slightly evolving with the growth of three shoulders at 1.5, 9.5 and 14.5 ppm (Figure 4). The tetrahedral peak also becomes gradually more structured with the growth of four shoulders at 77, 69, 59 and 50 ppm with progressive thermal treatment, at the expense of the line at 64 ppm.

The peak integrations at octahedral and tetrahedral shifts provides a quantitative ratio of IV:VI coordination of 32:68 without significant changes among the variously calcined sample (Table 1). The boehmite sample is characterized by a ratio 0:100. No pentahedral (Al^V) was detected for all samples.

The *in situ* XRD data are graphically summarized in Figure 5. The sample demonstrates a well-crystalline phase of boehmite at room temperature (RT, 30 °C). No detectable alterations are perceived in the diffraction pattern until the temperature reaches 450 °C. At 450 °C, the distinctive peaks of the boehmite structure (ICDD 00-005-0190) decrease in intensity and totally disappear at 500 °C. New peaks that can be attributed to the γ-Al_2O_3 phase appear. The observed broadening of the peaks associated with the γ-Al_2O_3 phase indicated a decrease in the size of crystalline domains and/or an increase in structural disordering that occurs during the phase transition. Between 850 and 950 °C a split of the peak at ~45.6° seems to indicate a structural change and a phase transition. Since the peaks are broad it could also be attributed to two narrow peaks splitting apart during the thermal treatment.

Starting at 1100 °C we observe the appearance and disappearance a series of peak that can be attributed to different phase transitions which indicates a mix of different phase: δ and θ Al_2O_3 between 1100 °C and at 1200 °C (first half an hour), θ and α Al_2O_3 between half an hour and 2 hours at 1200 °C and finally only α Al_2O_3 after 2 hours at 1200 °C.

The analysis of selected area electron diffraction (SAED) patterns displays analogous characteristics to that of X-ray diffraction (XRD) analysis with respect to phase transitions(Figure 6). The limitations of SAED data in providing comprehensive insights at the individual particle level should be noted, originating fromthe complexity in distinguishing between various transition alumina phases, the presence of mixed transition alumina phases, and the existence of aggregates. These challenged are particularly pronounced in such small crystallite, where individual crystals are difficult to analyze.

The morphological changes and local phase transformations detected from the TEM images and SAED patterns at various temperatures are depicted in Figure 6. The boehmite sample initially comprises regular and homogeneous variously truncated rhombohedral platelets with dimensions of nearly 40 nm

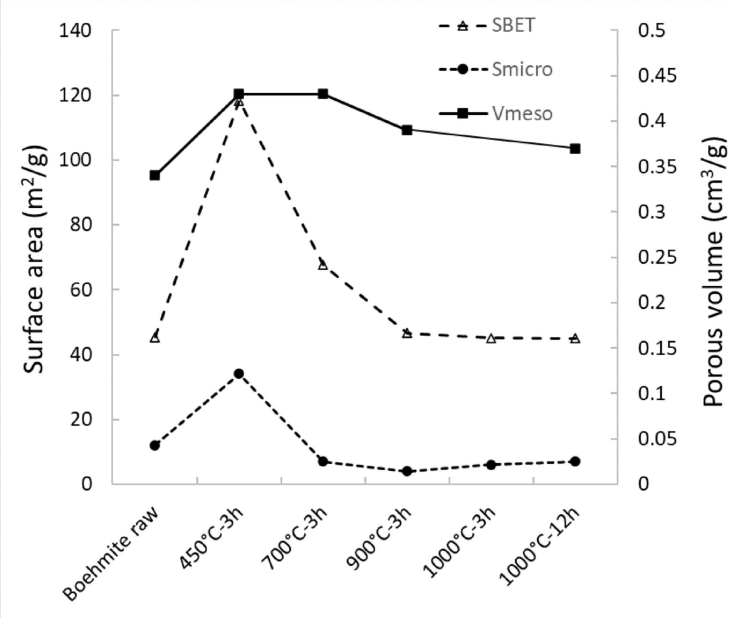

Figure 3. Textural analysis results for the BET surface area, the mesoporous volume (Hg porosimetry), and the microporous volume (N_2-physisorption t-plot) for the raw boehmite sample and the different calcination stages.

in their longest axis and thickness usually below 10 nm. There were no discernible alterations in morphology initially following exposure to a temperature of 100 °C for a duration of one hour. At temperatures exceeding 400 °C, visible alterations in texture become apparent, characterized by the appearance of pores measuring approximately 0.5–1 nm in length. Upon further elevation of temperature and a heating duration of 30 minutes, the pores undergo a transformation from their initial configuration to a morphology resembling slits, characterized by dimensions of 0.5–1.5 nm along the minor axis and 3–5 nm along the major axis. Due to better resolution in the absence of the gas phase, the pores are better visible in the *ex-situ* STEM images and have been marked for better visualization. Following the heating, the pores that were originally shaped like slits undergo a transformation into more faceted and equant shapes with dimensions of approximately 3–5 nm by 4–6 nm occurring at a temperature of ca. 800 °C. Further application of heat results in the growth of pores (4–6 nm in width and 6–8 nm in length) with stronger facetted morphologies. At a temperature of 1000 °C, the larger crystallites feature persistently facetted pores with dimensions ranging from 6–10 nm, in lesser number as in previous temperature steps. These pores are comparatively less abundant than those observed in earlier stages. In addition to the evolution of the pore population, two other morphological features are observed to evolve especially in the final prolonged 1000 °C step (Figure 7). First, on the large crystallites, the initial sharp rhombohedral shape is maintained without extensive alteration until the prolonged exposure to 1000 °C, where the sharpest angles of the rhombohedron suffers very noticeable smoothing or truncation, in the clearest cases at the favor of a newly formed facet orthogonal to the longest axis of the rhombohedron. Second, the smaller crystallite aggregates, which have a rather poor contrast in the *in-situ* STEM setup, have a systematic tendency to collapse and form smaller aggregates with less defined facetted morphologies.

The direct observation of the formation of the α-Al_2O_3 phase *in situ* was limited by the temperature constraints in the TEM holder and hence, in order to observe the morphology of the alpha phase, the sample issued from *in situ* XRD analysis was subsequently subjected to TEM study, as depicted in Figure 8. The particles under observation display a rounded, polylobate morphology, with dimensions spanning from 200–500 nm.

Ex situ TEM and STEM characterization were performed to confirm and refine the observations made *in situ*. Following a calcination process lasting 3 hours at 450 °C, the appearance of crystalline planes, namely (400), (440), and (222), which are indicative of γ-Al_2O_3, has been verified through electron diffraction data (Figure 9). Visible alterations to the surface of the platelets were observed with identical morphological aspects as those observed *in situ*, such as the presence slit-shaped pores in orientations orthogonal to the longest axis of the rhombohedron.

After undergoing a thermal treatment at a temperature of 1000 °C *ex situ* for a duration of 3 hours (Figure 10), the pores that were previously in the form of slits have grown and display a facetted morphology with equant facets, and in numerous occurrences, longest axis orthogonal to the longest axis of the rhombohedron. The findings from the electron diffraction measurements are consistent with those obtained from the *in-situ* X-ray diffraction measurements, suggesting the presence of a composite or blend of transition alumina phases within the crystallite aggregates (Figure 6–7,).

Upon subjecting the boehmite samples to a thermal treatment of 1000 °C for a duration of 12 hours, significant observations were made with respect to the existence of pores as shown in Figure 11. A progressive reduction in the quantity

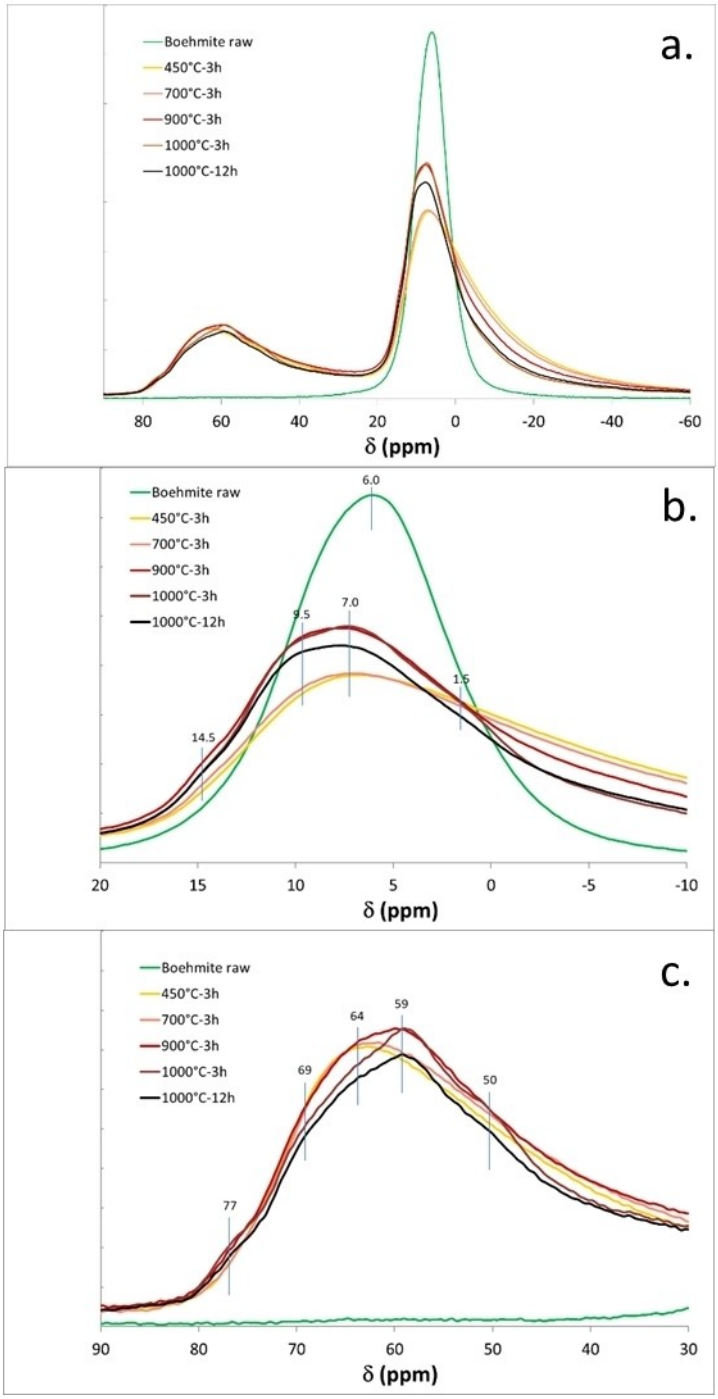

Figure 4. ^{27}Al MAS NMR spectra for the initial boehmite and samples calcined up to 1000 °C for 12 h. (a) full spectra. (b) is a focus on the octahedral contributions, (c) on the tetrahedral contributions.

of pores can be observed, accompanied with a transition towards a more facetted morphology as observed from *in-situ* experiments. The morphological smoothing of the individual crystallites and aggregates is clearly evidenced.

Discussion

Bulk Structural Evolution

The literature regarding the structural evolution of transition alumina is extensive but does not easily converge on a single scheme.[42] It is clear from previous work that the structural evolution of alumina through calcination from hydroxide and oxyhydroxide percursors depends on the crystallite size of the

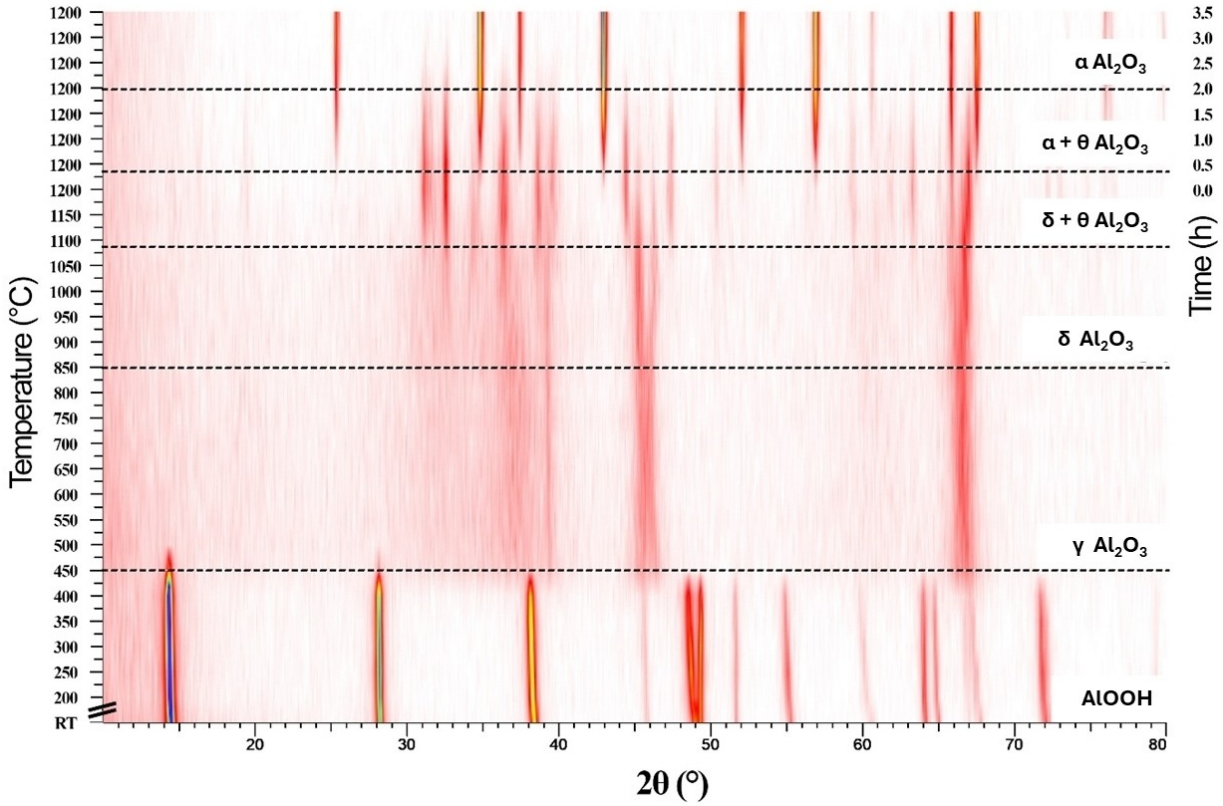

Figure 5. (a) X-ray diffractograms in function of temperature during the calcination of boehmite to α-Al_2O_3 from 30 °C (RT) to 1200 °C with an isothermal hold for 4 h at 1200 °C. (b) 2D representation of the same data.

initial hydroxylated phases, the concentration of impurities (sodium) and the temperature program employed (time-temperature couple).[1,43] Furthermore, the different characterization methods used over the last three decades suffer from inconsistencies that underline the technical progress made in this time frame, more specifically regarding solid state NMR.[21,42–44] While resolving the structure of the different alumina phases is beyond the scope of this study, it is important to properly assign the different samples obtained to the known stages of structural evolution. The *in situ* XRD and ^{27}Al NMR data are consistent with the existing literature under equivalent time-temperature conditions of boehmite calcination,[35,45–47] particularly on low specific surface area samples (e.g. large crystallites). The sharp formation of the γ-Al_2O_3 phase at 450 °C with characteristic diffuse diffraction peaks coevals with the complete loss of the boehmite pattern indicates a sharp phase transition along the heating program, consistent with the sharp mass loss measured in TGA in the 400–450 °C range. The value and constancy of the tetrahedral to octahedral ratio in the transition alumina obtained by NMR is consistent with previous observations among γ- and δ-Al_2O_3 with similar crystallite morphologies.[48] γ- and δ-Al_2O_3 were shown to bare essentially the same Al and O sublattices but with varying cationic disorder.[43,49]

The sharpening and multiple shouldering of the NMR data from 700 °C to 900 °C indicate a loss of disorder from the initial γ-Al_2O_3 phase at 450 °C, with progressive cation mobility to consistent tetrahedral and octahedral sites in the δ-Al_2O_3 phase.[48] This is supported by the constant tetrahedral to octahedral ratio in the *ex-situ* samples and the increased order seen in the sharpening XRD patterns and NMR spectra. These changes suggest a progressive occupancy of tetrahedral and octahedral sites, as detailed by Chandran et al. (2019) and Xu et al. (2021)[48,49] using multidimensional ^{27}Al experiments at high magnetic fields. These configurations converge towards that of the pure δ-Al_2O_3 phase until the transition to θ-Al_2O_3. The phase transition, marked by specific peak features in the ^{27}Al NMR spectra, is absent in our *ex-situ* data, aligning with the *in situ* XRD data showing θ-Al_2O_3 only appears from 1100 °C. This is 100 °C above the calcination temperature of the most sever *ex situ* sample. This indicates that, between 450–1000 °C, Al^{3+} environments reorganize from a disordered state towards tetrahedral and octahedral coordination typical of the δ- Al_2O_3 phase.

Morphological Evolution of Individual Crystallites

Beyond the apparent morphological similarity of crystal morphologies between boehmite and transition alumina resulting from the topotactic/pseudomorphic transformation, morphological disorder is evident from the number of pores and the roughness of the crystals' external surfaces. The pores number, size, and shape indicate a dynamic structural reorgan-

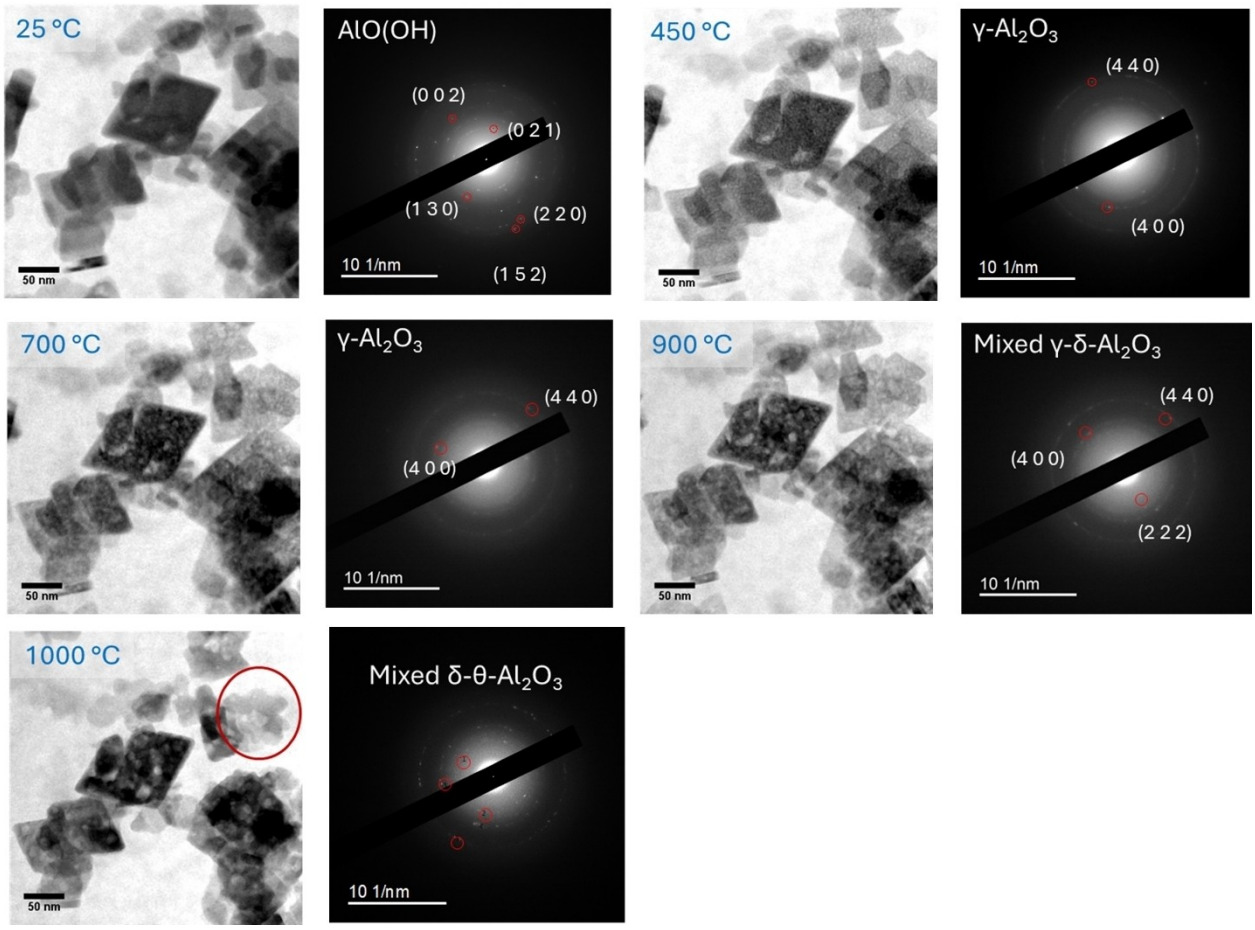

Figure 6. Bright-field images and their corresponding SAED patterns of the same region monitored during the calcination of boehmite from room temperature to 1000 °C.

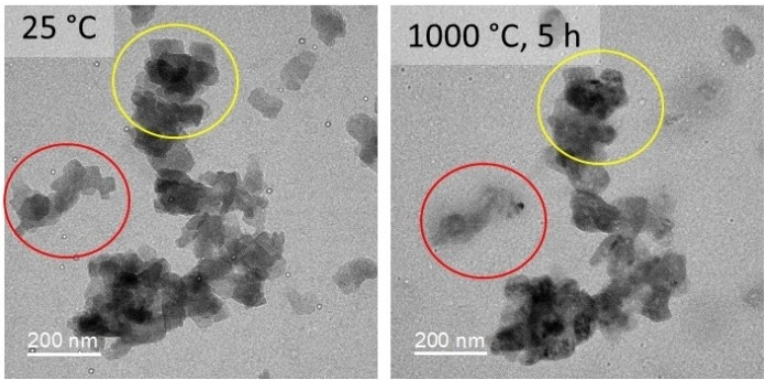

Figure 7. TEM images of the same chosen area at 25 °C and after 5 hours of heating at 1000 °C.

ization at the mesoscale, transitioning from numerous slit-like pores (~1 nm opening) at 450 °C to fewer, facetted pores (~5 nm) at 1000 °C.

The morphological evolution of the pores is further evidenced by the changes in porous volume and specific surface area measured by Hg-porosimetry and N_2-physisorption. The most disordered phase, the 450 °C calcined sample, shows the highest meso and microporous surfaces and volumes, more than doubled than that of the initial boehmite. The decrease in the intermediate size range (10–20 nm) mesopore in favor of the larger mesopores (40–50 nm) at 1000 °C indicates pore coalescence and crystallite contraction. In the micropore domain, the sharp disappearance of micropores (0.35–0.5 nm) at temperatures higher than 600 °C suggests either structural collapse around microporous slits in early calcination stages or the opening of the micropores to mesoporous scales through

Research Article
doi.org/10.1002/cctc.202400677
Chemistry Europe
European Chemical Societies Publishing

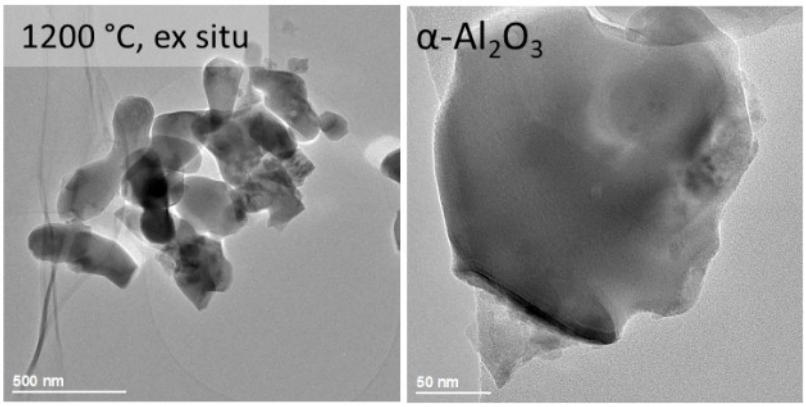

Figure 8. TEM observation of the α-Al_2O_3 phase collected after the in situ XRD analysis.

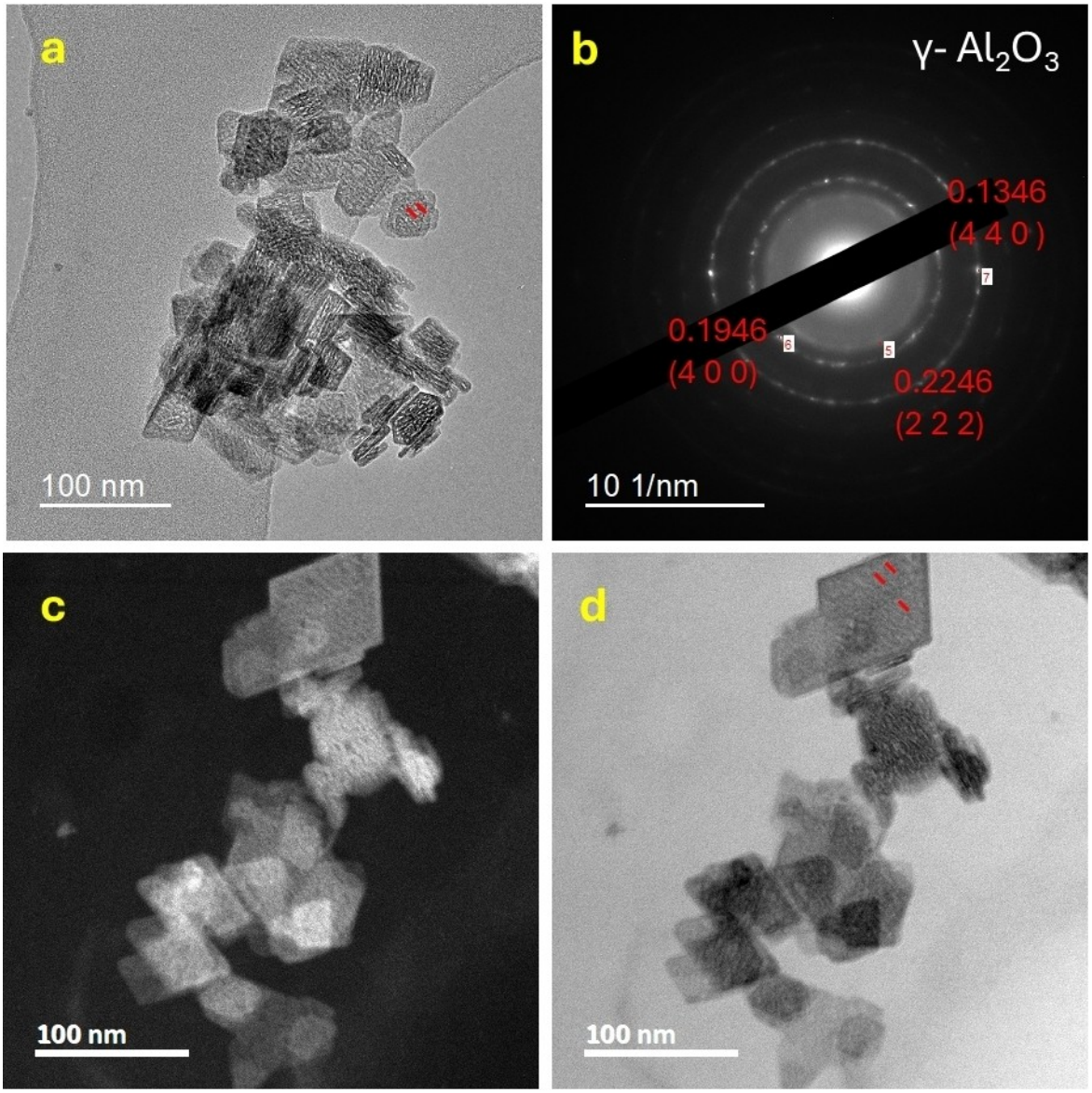

Figure 9. (a) TEM images, (b) electron diffraction patterns, (c) STEM dark field image and (d) STEM bright field image of γ-Al_2O_3 from boehmite that was calcined at 450 °C for 3 hrs. Red lines on figure (a) and (d) represents the slit-like pore forming perpendicular to the longest axis.

Research Article
doi.org/10.1002/cctc.202400677
Chemistry Europe
European Chemical Societies Publishing

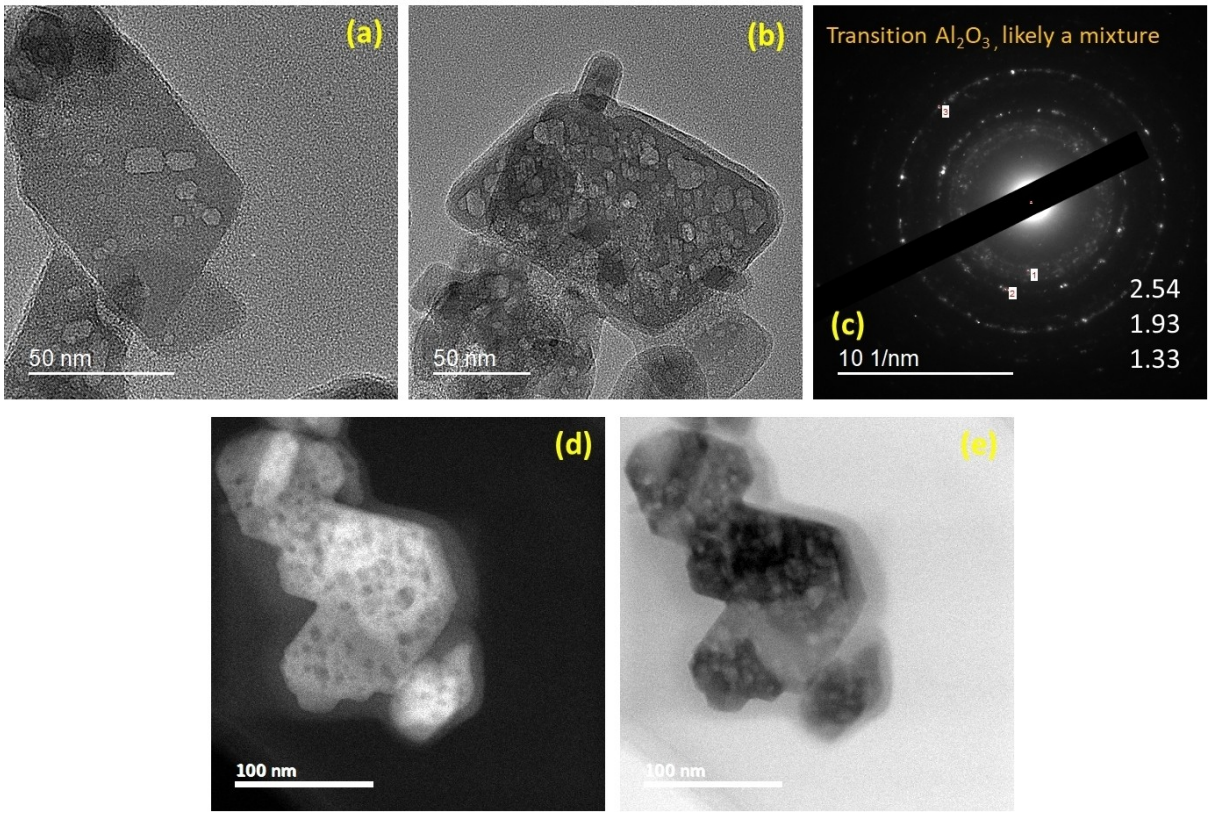

Figure 10. (a and b) TEM images of δ/Θ-Al_2O_3 from boehmite that was calcined at 1000 °C for 3 hrs, (c) electron diffraction patterns of the obtained transition alumina, (d and e) corresponding STEM dark field and bright field images obtained.

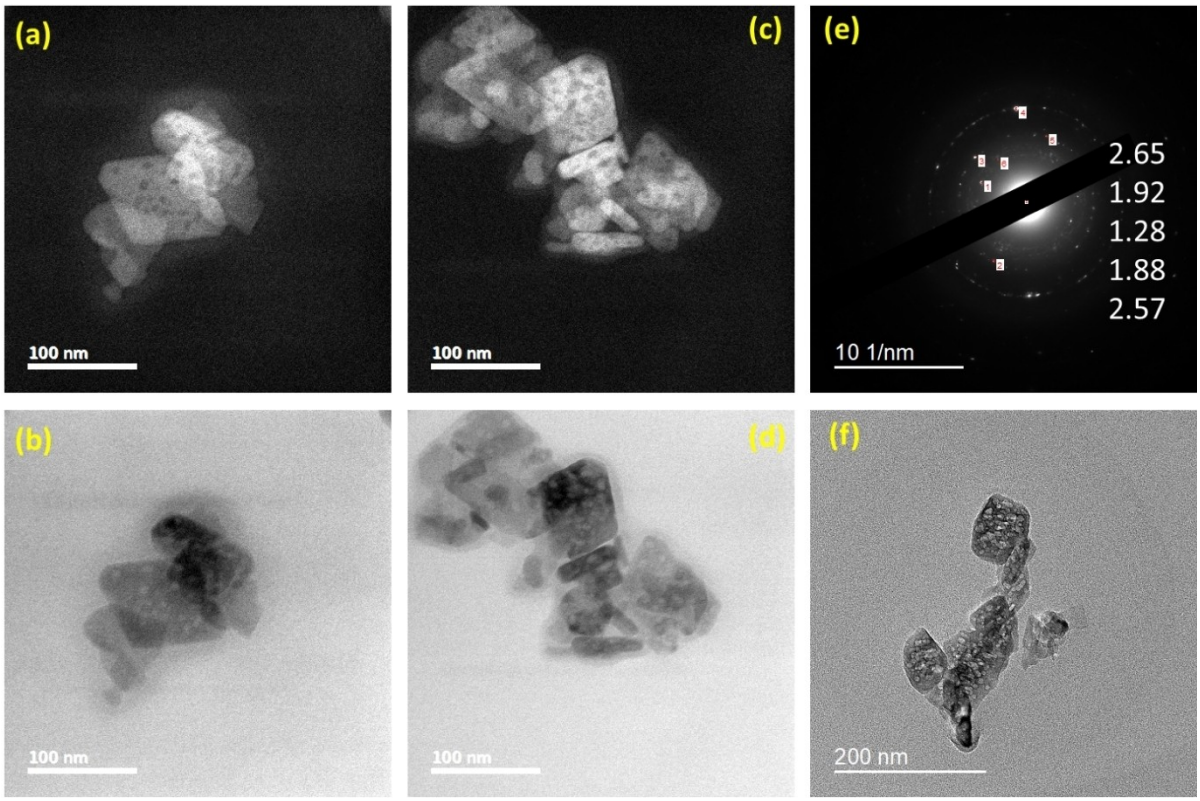

Figure 11. (a–d) STEM dark field and bright field images of δ/Θ- Al_2O_3 from boehmite that was calcined at 1000 °C for 12 hrs, (e) electron diffraction patterns of the obtained transition alumina, (f) TEM images of the final phase.

coalescence. While structural collapse cannot be entirely dismissed, evidence strongly supports coalescence process. Similar observations of micropore formation and subsequent obliteration, along with mesopore increase have been discussed early by Wilson et al. (1981)[1] and later Paglia et al. (2004)[8] reaching similar conclusions for micron sized crystals.

Additionally, pore morphology analysis from STEM and TEM images demonstrates an increase in mesopore size during the transition from slit-like to equant pores in both γ-Al_2O_3 and δ-Al_2O_3 phases.[32,50,51] Wilson et al.[1] found that during the topotactic transformation of AlOOH to γ-Al_2O_3, large crystallite exhibited a lamellar slit-shaped configuration with widths of approximately 18 Å, oriented perpendicularly to the basal (010) plane of boehmite. These pores were uniform in orientation and inter-pore distances, typically ranging from 35–40 Å. The mechanism for their formation resembles to that observed during the dehydration of isostructural γ-FeOOH, suggesting a collapse mechanism leading to a spinel-like structure within the undecomposed matrix of γ-FeOOH.[52] Wilson et al.[1] argues that a collapse process involving internal proton and hydroxyl condensation to remove water between layers is structurally plausible, independent of the pore formation. Additionally, a novel theory proposes that lamellar pores form through diffusion-controlled proton migration and counter diffusion of aluminum cations, facilitating the γ-Al_2O_3 structure.[20,53,54] This process aligns with the movement of boehmite layers required for interlayer site development and a face-centered cubic oxygen lattice.[55]

In this study, the pore morphology tends towards a polyhedral negative crystal morphology (a void that has a morphology bound by walls oriented according to the crystal lattice of the mineral that hosts it) that keeps an anisotropic character which is often orthogonal to the longest axis of the hosting crystal. Boehmite crystal which are shaped like lozenge platelets are bound by $(101)_b$ lateral faces and $(010)_b$ basal planes (b for boehmite). Initially, slit-like pores tend to develop their long axis in the $(001)_b$ plane visible in the $(010)_b$ zone axis, as well as along the $(010)_b$ plane visible through lateral facet zone axes. Upon further heating, pores developing in the $(010)_b$ plane tend to increase their $(101)_b$ edges while maintaining their maximum dimensions in the $(001)_b$ plane (Figure 12). This mechanism drives the pore morphology towards negative crystals with morphologies differing from that of initial boehmite crystals.

Observation of these pores is optimal along the $(010)_b$ zone axis, which presents a flat projection of the basal plane, complicating surface reconstruction analysis. The possibility of local reconstruction with other index faces on the apparent $(010)_b$ surfaces of pores cannot be excluded. This pore formation mechanism aims to minimize crystal surface energy by favoring terminations with the lowest energy under the calcination conditions and structure of the transition alumina. According to recent DFT calculations by Pigeon et al. (2022),[19] surface termination energies favor the $(001)_a$ orientation (as for alumina) under the study's relevant temperature conditions. The sequence of pore shaping observed here aligns with this energy hierarchy, starting with $(001)_b$ (topotactic to $(001)_a$), followed by $(010)_b$ (topotactic to basal $(110)_a$), and then $(111)_b$ (topotactic to $(111)_a$). This pore morphology has been well-documented by Kovarik et al. (2013)[56] using electron tomography on gamma alumina crystals derived from boehmite calcined at 800 °C. Their study ranked surface energies as $(100)_a \leq (111)_a < (110)_a$ for similar morphologies.

The structural disorder inherited from the boehmite structure collapse is accompanied by substantial retention of protons, which has been shown by several authors through detailed FTIR and 1H NMR experiments.[8,15,32,54] Such protons have been described as representative of surface terminations of the alumina structure, with a debated fraction of hydrogen retention related to amorphous regions and/or to an internal occluded porosity. The gradual loss of mass in the 450 °C–850 °C observed with TGA (Figure 1), correlated with the diminution of the specific surface area within this temperature range correlates well with a gradual loss of the number of hydroxylated surface terminations.

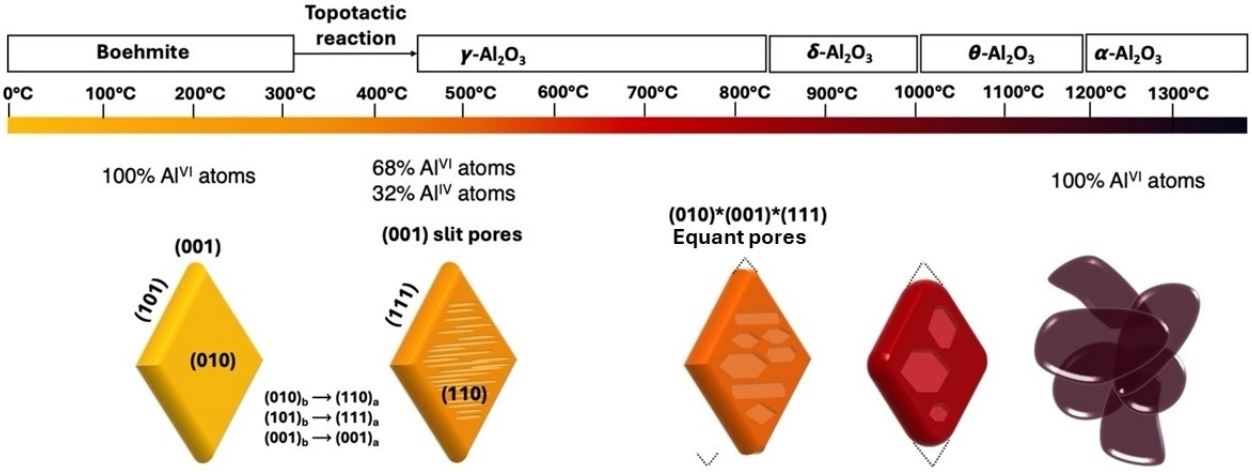

Figure 12. Schematic representation of the crystallite morphological evolution with progressive calcination.

Conclusions

The calcination of boehmite crystal with rhombohedral platelet crystallite shapes with 40 nm sizes has been performed in air from ambient to 1000 °C and monitored in real time by *in situ* XRD and *in situ* TEM experiments. The *in situ* XRD shows the sharp appearance of γ-Al_2O_3 at 400 °C at the collapse of boehmite and its progressive dehydration from 400 to 450 °C evidenced by TGA. δ-Al_2O_3 appears at the expense of γ-Al_2O_3 at 820 °C, itself later replaced by θ-Al_2O_3 from 1000 °C until the formation of α-Al_2O_3 initiated at 1200 °C. The ^{27}Al MAS NMR data indicate the conversion of 32% of octahedral sites into tetrahedral sites upon dehydration of boehmite which remains constant throughout the heating up to 1000 °C for 12 h. The sharpening and modulations in the NMR octahedral and tetrahedral peaks are consistent with the progressive ordering of the cationic sites from an initial highly disordered γ-Al_2O_3. Nitrogen physisorption and mercury porosimetry data point to the appearance at 450 °C of 4–20 nm mesopores and micropores which gradually disappear at 600 °C and 900 °C and are fully destroyed at the benefit of larger mesopores in the 40–50 nm range. This micro/mesoporous evolution is clearly visible in *in situ* TEM experiments, together with control *ex situ* experiments. The pore morphology in the initial γ-Al_2O_3 step after boehmite dehydration is characterized by sub-nanometer wide slit shapes preferentially oriented in the (001) plane which is orthogonal to the basal plane (110) and to the longest axis of the crystallites rhombus shapes. Further heating across the δ-Al_2O_3 transition induces the development of the basal (110) surface and of the (111) faces in the pore morphology which converge towards equant platelet shapes. The number of pores is also seen to decrease while their sizes gradually increase up to 10 nm after heating at 1000 °C. Finally, the crystallite morphology after heating at 1000 °C for 12 h shows visible effects of rhombohedral truncation at (111) surface intersections by (001) directions, and general sintering of small crystallite aggregates. The morphology hence gradually evolves from a highly disordered initial state of abundant slit-like pores towards a reduced population of larger pores with a negative crystal morphology likely exposing a minimal surface energy configuration. This pore morphology evolution reasonably agrees with the stability of specific γ-Al_2O_3 surfaces calculated recently. The structural changes visible in ^{27}Al MAS NMR and XRD indicate that cation mobility gradually allows for removing disorder by achieving specific cationic positions in tetrahedral and octahedral coordinations at discrete phase transformation events. At the light of these results, we emphasize on the importance of tracking correlated changes in structural and morphological properties of nanocrystal in such topotactic/pseudomorphic reactions, which provides crucial information for the understanding of the thermodynamics and kinetics of nanoscopic phase transformation.

Acknowledgements

This work is conducted within the framework of the Laboratoire Commun de Recherche de Caractérisation des Matériaux pour les énergies Nouvelles - LCR Carmen (Characterization of Materials for new Energy) collaboration between IFPEN, CNRS, University of Strasbourg, ENS Lyon, University of Lyon, and Sorbonne University, Paris. It is funded by IFP Energies Nouvelles as part of NS's PhD thesis. The authors express gratitude to the DRX and MET platforms of IPCMS, as well as R05 - Direction Physique et Analyse of IFP Energies Nouvelles, for their provision of adequate research facilities for the successful completion of this study. The authors would like to express their gratitude to Dr. Nathalie SCHILDKNECHT, the Director of the CARMEN Joint laboratory, for her consistent and unwavering guidance during the completion of this study.

Conflict of Interests

The authors declare no conflict of interest.

Data Availability Statement

The data that support the findings of this study are available from the corresponding author upon reasonable request.

Keywords: transition alumina · porous alumina · boehmite transformation · thermal processing · structural transition · topotactic transformation · morphology-structure correlation · in situ study · transmission electron microscopy

[1] S. J. Wilson, *J. Solid State Chem.* **1979**, *30*, 247–255.
[2] P. Euzen, et al., in *Handbook of Porous Solids 1591–1677*. Wiley, **2002**. doi: 10.1002/9783527618286.ch23b.
[3] M. L. Guzmán-Castillo, X. Bokhimi, A. Toledo-Antonio, J. Salmones-Blásquez, F. Hernández-Beltrán, *J. Phys. Chem. B* **2001**, *105*, 2099–2106.
[4] G. FU, et al., *Trans. Nonferr. Met. Soc. China* **2010**, *20*, s221–s225.
[5] P. Alphonse, M. Courty, *Thermochim. Acta* **2005**, *425*, 75–89.
[6] M. Mohammadi, M. Khodamorady, B. Tahmasbi, K. Bahrami, A. Ghorbani-Choghamarani, *J. Ind. Eng. Chem.* **2021**, Preprint at https://doi.org/10.1016/j.jiec.2021.02.001.
[7] Q. Liu, et al., *Microporous Mesoporous Mater.* **2008**, *111*, 323–333.
[8] G. Paglia, et al., *Chem. Mater.* **2004**, *16*, 1914–1923.
[9] C. Wolverton, K. C. Hass, *Phys. Rev. B* **2000**, *63*, 024102.
[10] C. Legros, C. Carry, P. Bowen, H. Hofmann, *J. Eur. Ceram. Soc.* **1999**, *19*, 1967–1978.
[11] R. A. Shelleman, G. L. Messing, M. Kumagai, *J. Non Cryst. Solids* **1986**, *82*, 277–285.
[12] K. Wefers, C. Misra, *Oxides and Hydroxides of Aluminum. Alcoa Technical Paper No. 19. Aluminum Company of America*, **1987**, *92*, 20–23.
[13] K. Wefers, *Alumina Chemicals: Science and Technology Handbook*. The American Ceramic Society, Westerville, Ohio, **1990**.
[14] T. Tsukada, H. Segawa, A. Yasumori, K. Okada, *J. Mater. Chem.* **1999**, *9*, 549–553.
[15] L. Kovarik, et al., *J. Phys. Chem. C* **2014**, *118*, 18051–18058.
[16] A. Boumaza, et al., *J Solid State Chem* **2009**, *182*, 1171–1176.
[17] M. GUZMANCASTILLO, *J Non Cryst Solids* **2003**, *329*, 53–56.
[18] P. Palmero, et al., *Int J Appl Ceram Technol* **2009**, *6*, 420–430.
[19] T. Pigeon, C. Chizallet, P. Raybaud, *J Catal* **2022**, *405*, 140–151.
[20] Z. Luo, *Acta Crystallogr B Struct Sci Cryst Eng Mater* **2021**, *77*, 772–784.
[21] A. R. Ferreira, et al., *J Solid State Chem* **2011**, *184*, 1105–1111.

[22] G. Busca, *Catal Today* **2014**, *226*, 2–13.
[23] R.-S. Zhou, R. L. Snyder, *Acta Crystallogr B* **1991**, *47*, 617–630.
[24] M. Digne, *J Catal* **2004**, *226*, 54–68.
[25] X. Liu, *J. Phys. Chem. C* **2008**, *112*, 5066–5073.
[26] M. Digne, P. Sautet, P. Raybaud, P. Euzen, H. Toulhoat, *J. Catal.* **2002**, *211*, 1–5.
[27] M. F. Peintinger, M. J. Kratz, T. Bredow, *J. Mater. Chem. A* **2014**, *2*, 13143–13158.
[28] R. Prins, *J. Catal.* **2020**, *392*, 336–346.
[29] G. N. Kryukova, D. O. Klenov, A. S. Ivanova, S. V. Tsybulya, *J Eur Ceram Soc* **2000**, *20*, 1187–1189.
[30] M. Rudolph, M. Motylenko, D. Rafaja, *IUCrJ* **2019**, *6*, 116–127.
[31] L. Kovarik, et al., *Angew. Chem. Int. Ed.* **2020**, *59*, 21719–21727.
[32] L. Kovarik, M. Bowden, J. Szanyi, *J. Catal.* **2021**, *393*, 357–368.
[33] B. C. Lippens, J. H. de Boer, *Acta Crystallogr.* **1964**, *17*, 1312–1321.
[34] S. J. Wilson, J. D. C. McConnell, M. H. Stacey, *J. Mater. Sci.* **1980**, *15*, 3081–3089.
[35] G. Paglia, et al., *Phys. Rev. B Condens. Matter. Mater. Phys.* **2003**, *68*, 144110.
[36] G. Paglia, A. L. Rohl, C. E. Buckley, J. D. Gale, *Phys Rev B* **2005**, *71*, 224115.
[37] G. Paglia, et al., *Boehmite-Derived γ -Alumina System. 2. Consideration of Hydrogen and Surface Effects*. 1914–1923, **2004**. doi:10.1021/cm035193e.
[38] Sasol Performance Chemicals. *DISPERAL DISPAL Content High-Purity Dispersible Alumina Hydrates Content*. https://products.sasol.com/pic/products/home/grades/EU/5disperal-and-dispal/index.html, **2019**.
[39] P. Alphonse, M. Courty, *Thermochim. Acta* **2005**, *425*, 75–89.
[40] A. Boumaza, et al., *J. Solid. State Chem.* **2009**, *182*, 1171–1176.
[41] M. Rudolph, et al., *Adv Eng Mater* **2017**, *19*, 1700141.
[42] L. Kovarik, M. Bowden, K. Khivantsev, J. H. Kwak, J. Szanyi, *Acta Mater.* **2024**, *266*, 119639.
[43] C. Pecharromán, I. Sobrados, J. E. Iglesias, T. González-Carreño, J. Sanz, *J. Phys. Chem. B* **1999**, *103*, 6160–6170.
[44] C. Vinod Chandran, et al., *Chem. Soc. Rev.* **2019**, *48*, 134–156.
[45] B. K. Gan, I. C. Madsen, J. G. Hockridge, *J. Appl. Crystallogr.* **2009**, *42*, 697–705.
[46] S. Lamouri, et al., *Boletín de la Sociedad Española de Cerámica y Vidrio* **2017**, *56*, 47–54.
[47] G. Urretavizcaya, A. L. Cavalieri, J. M. P. López, I. Sobrados, J. Sanz, *J. Mater. Synth. Process.* **1998**, *6*, 1–7.
[48] S. Xu, et al., *ACS Omega* **2021**, *6*, 4090–4099.
[49] C. V. Chandran, et al., *Chem. Soc. Rev.* **2019**, *48*, 134–156.
[50] L. Kovarik, et al., *Chem. Mater.* **2015**, *27*, 7042–7049.
[51] L. Kovarik, M. Bowden, D. Shi, J. Szanyi, C. H. F. Peden, *J. Phys. Chem. C* **2019**, *123*, 9454–9460.
[52] R. Giovanoli, R. Brütsch, *Thermochim. Acta* **1975**, *13*, 15–36.
[53] X. Krokidis, et al., *J. Phys. Chem. B* **2001**, *105*, 5121–5130.
[54] G. Paglia, et al., *Chem. Mater.* **2004**, *16*, 220–236.
[55] R. Giovanoli, R. Brütsch, *Thermochim. Acta* **1975**, *13*, 15–36.
[56] L. Kovarik, et al., *J. Phys. Chem. C* **2013**, *117*, 179–186.

Manuscript received: April 11, 2024
Revised manuscript received: June 23, 2024
Accepted manuscript online: July 2, 2024
Version of record online: September 4, 2024